J. Fluid Mech. (1968), *vol.* 33, *part* 2, *pp.* 303–319
Printed in Great Britain

Velocity gradients at the wall for flow around a cylinder for Reynolds numbers between 60 and 360

By HARRY G. DIMOPOULOS† AND THOMAS J. HANRATTY

Department of Chemistry and Chemical Engineering,
University of Illinois, Urbana, Illinois

(Received 13 November 1967)

This paper shows how electrochemical techniques can be used in studies of flow around solid objects to measure the velocity gradient at the solid boundary. The method holds the advantages that it is not necessary to calibrate and that the test element is easy to fabricate. A study of the distribution of the wall velocity gradient around a cylinder of 1 in. diameter indicates that boundary-layer theory correctly predicts the measurements between the front stagnation point and the separation for Reynolds number, R, greater than 150. The wall velocity gradients in the wake are much smaller than in the front part of the cylinder and they reveal a minimum which is quite close to the separation point.

1. Introduction

The prediction of the velocity gradient at a boundary has been one of the main goals of theoretical studies of flow around solid objects, yet, very few direct measurements of this quantity have been obtained. Some of the techniques that have been used or that have been suggested for use include velocity measurements close to the surface, thermal meters, stress plates, and surface tubes (Bellhouse & Shultz 1966). These methods are difficult to apply either because of the smallness of the boundary-layer thickness compared to the size of the measuring instrument or because of the need to calibrate.

Reiss & Hanratty (1962, 1963) and Mitchell & Hanratty (1966) have recently shown how electrochemical techniques may be used to measure the time averaged and the fluctuating velocity gradient at the wall for turbulent flow in a pipe. A chemical reaction is carried out at the surface of a small electrode embedded in the wall. If the voltage applied to the electrodes is large enough, the current flowing in the circuit is controlled by the mass transfer rate and the electrode is said to be polarized. The test electrode can be made quite small so that the concentration boundary layer over the electrode surface is small compared to the velocity boundary layer. Under these circumstances the current flowing in the circuit when the test electrode is polarized is related to the local velocity gradient at the wall. This electrochemical technique is the mass transfer analogue of the thermal meter already used by a number of investigators. However, it holds advantages

† Present address: Shell Pipeline Corporation, Houston, Texas.

over the thermal meter in that it is not necessary to calibrate and in that the test element is easier to fabricate.

Therefore it was decided to examine the usefulness of electrochemical techniques in more general applications than pipe flow. The flow around a circular cylinder has been investigated both with and without a splitter plate in the wake.

This paper reports on results obtained over the Reynolds number range of 60 to 360. A study at higher Reynolds numbers conducted in this laboratory by Son (1968) will be described in a later paper.

To the knowledge of the authors the results of this study and those of Son are the only direct measurements of the distribution of the wall velocity gradient around a cylinder that have been reported, other than the measurements with surface tubes by Fage and Falkner over a Reynolds number range of 10^5 to 10^6 (see Goldstein 1938, p. 427). Bellhouse & Schultz (1966) used a thermal meter to study flow around a cylinder but they did not calculate velocity gradient from their thermal measurements. The results of this study are of interest in that they allow a direct examination of the validity of boundary-layer theory and in that they reveal some aspects of the flow in the wake.

Experiments were also conducted for which the reaction was occurring over the entire surface of the cylinder. Measurements at the test electrode then revealed the local mass transfer rate. The comparison of these mass transfer measurements with calculations based on the measured velocity gradients was helpful in evaluating the accuracy of the experiments.

2. Calculation of velocity gradient at a wall

The method for relating the mass transfer rate to the velocity gradient at the boundary will now be presented.

Consider a rectangular electrode embedded in the surface of a cylinder with its long side perpendicular to the direction of the flow. The width of the electrode is so much greater than the length L that the concentration boundary layer may be considered as two-dimensional. Consider a co-ordinate system for which the x co-ordinate is tangent and the y co-ordinate is perpendicular to the surface. The reaction which occurs at the surface of the test electrode is

$$\mathrm{Fe(CN)}_6^{-3} + e^- \rightarrow \mathrm{Fe\,(CN)}_6^{-4}. \tag{1}$$

Since the reaction is carried out in the presence of a large excess of sodium hydroxide, the mass balance for the ferricyanide ion $[\mathrm{Fe(CN)_6}]^{-3}$ is given as

$$u\frac{\partial c}{\partial x} + v\frac{\partial c}{\partial y} = D\frac{\partial^2 c}{\partial y^2}. \tag{2}$$

The reaction at the surface of the electrode proceeds at such a rapid rate that $c = 0$ at $y = 0$. The other two boundary conditions are $c(x, \infty) = c(0, y) = c_B$.

Because of the small length of the electrode and the small diffusion coefficient of the ferricyanide ion, the concentration boundary layer over the electrode

surface is very thin compared to the velocity boundary layer. The following approximations may therefore be made for the velocity field:

$$u = \beta(x)\, y, \quad v = -\frac{1}{2}\frac{d\beta}{dx} y^2. \tag{3}$$

The quantity $\beta(x)$ is the velocity gradient at the surface. After substituting u and v and using a similarity transformation (Acrivos 1960) (2) may be solved to give the concentration gradient at some location on the electrode surface

$$\left(\frac{\partial c}{\partial y}\right)_{\text{wall}} = \left(\frac{1}{9D}\right)^{\frac{1}{3}} \frac{c_B}{0{\cdot}893} \frac{\{\beta(x)\}^{\frac{1}{2}}}{\left[\int_0^x \{\beta(x)\}^{\frac{1}{2}}\, dx\right]^{\frac{1}{3}}}. \tag{4}$$

Except for a region in the vicinity of the front stagnation point ($\theta < 5°$) the variation of $\beta(x)$ over the surface of the electrode may be neglected. Therefore $\beta(x) = \beta_0$ and (4) can be integrated from 0 to L to give the average value of the mass transfer coefficient k over the electrode

$$\frac{\langle k \rangle L}{D} = \frac{1}{c_B} \int_0^L \left.\frac{\partial c}{\partial y}\right|_{y=0} dx, \tag{5}$$

$$\frac{\langle k \rangle L}{D} = 0{\cdot}807\, Z^{\frac{1}{3}}. \tag{6}$$

The dimensionless wall shear stress, Z, is defined by the relation

$$Z = \tau_0 L^2/\mu D \tag{7}$$

where τ_0 is the local shear stress, μ is the fluid viscosity.

Equation (6) is in error because of two simplifying assumptions made in deriving the mass balance equation (2), i.e. the neglecting of diffusion in the x-direction and of natural convection caused by density variations in the concentration boundary layer. The effect of these two simplifying assumptions will be examined separately.

Ling (1962) calculated by a finite difference scheme the heat transfer to a small strip on an insulated boundary which is located in a uniform shear field. He subdivided the strip into three zones: the leading edge, the trailing edge, and the zone between where a similarity solution is applicable. The additional contribution of the edges to the transfer caused by streamwise diffusion is given as $0{\cdot}19Z^{-\frac{1}{6}}$.

The combined effect of forced and free convection on boundary-layer flows has been studied by Acrivos (1966) and he proposes the following equation:

$$\xi(\zeta) = \xi_0 + 1{\cdot}26K \frac{\left[\int_0^\zeta \{\xi(\zeta)\}^{\frac{1}{2}} d\zeta\right]^{\frac{1}{3}}}{\{\xi(\zeta)\}^{\frac{1}{2}}} \sin(\theta), \tag{8}$$

where

$$\zeta = x/L, \tag{9a}$$

$$K = G_L/R_L^2 Sc^{\frac{1}{3}}, \tag{9b}$$

$$\xi(\zeta) = \frac{L}{u_\infty (R_L)^{\frac{1}{2}}} \beta(\zeta). \tag{9c}$$

For pure forced convection $\xi(\zeta) = \xi_0$. The Schmidt number Sc is the ratio of the kinematic viscosity to the diffusion coefficient. The Reynolds number R_L and

the Grashof number G_L are defined using the length of the electrode L as the length parameter.

For small values of K, (8) can be expanded as a power series in K. If this series is substituted into (4) the following expression is obtained for small K

$$\frac{\langle k\rangle L}{D} = 0{\cdot}807Z^{\frac{1}{3}} + 0{\cdot}253\frac{G_L}{R_L}\left(\frac{Sc}{Z}\right)^{\frac{1}{3}}\sin\theta, \tag{10}$$

where θ refers to the electrode position with respect to the front stagnation point.

If the effects of natural convection and streamwise diffusion are small then it seems reasonable to neglect their interaction and the combined corrections may be represented by the following equation:

$$\frac{\langle k\rangle L}{D} = 0{\cdot}807Z^{\frac{1}{3}} + 0{\cdot}19Z^{-\frac{1}{3}} \pm 0{\cdot}253\frac{G_L}{R_L}\left(\frac{Sc}{Z}\right)^{\frac{1}{3}}\sin\theta, \tag{11}$$

where + applies to aiding flows and − applies to opposing flows.

From Faraday's law the current I flowing in the electrochemical circuit can be related to $\langle k\rangle$ through the expression

$$\langle k\rangle = I/FAc_B, \tag{12}$$

where F is Faraday's constant and A is the area of the test electrode.

The dimensionless shear stress Z was calculated from the measured current I by means of (11) and (12).

The two correction terms in equation (11) were found to be important only at the lowest Reynolds numbers and near the separation point where Z is very small. For example, the correction was not greater than 2·7% anywhere on the surface of the cylinder at $R = 339$. At $R = 104$ the correction amounted to 27% at $\theta = 130°$ and to 14% at $\theta = 110°$ and to less than 10% at all other locations.

3. Description of experiments

Experiments were conducted with cylinders of 1 in. diameter in a one foot by one foot test section. The cylinder axis was perpendicular to the free stream. The splitter plate that was used in some of the runs was 4 in. long and 0·025 in. thick with a tapered leading edge. It was located two diameters downstream of the rear stagnation point of the cylinder.

The test section was in the gravity flow tunnel shown in figure 1. The tunnel was fabricated from Plexiglas, the piping of PVC plastic, and the pump of stainless steel. The tubes in the heat exchanger were Karbate. Nitrogen gas was purged into the system so that the fluid did not come into contact with air. A more detailed description of the construction of the tunnel and of the experiments is in a thesis by Dimopoulos (1968).

Two types of cylinders having diameters of 1 in. were fabricated. The one used for velocity gradient measurements had a platinum electrode, 0·020 in. wide × 0·500 in. long, embedded spanwise in a Plexiglas surface. The cylinder used in mass transfer studies had a round 0·020 in. platinum test electrode embedded in, but isolated from, the main electrode which covered an entire cylinder section. The two cylinders could be rotated while they were in the test section

so the position of the test electrodes with respect to the front stagnation point could be varied.

The electrolyte that was circulated through the tunnel had 0·01 molar concentrations of potassium ferrocyanide and potassium ferricyanide and a 1 molar concentration of sodium hydroxide. It was purged with nitrogen for about an

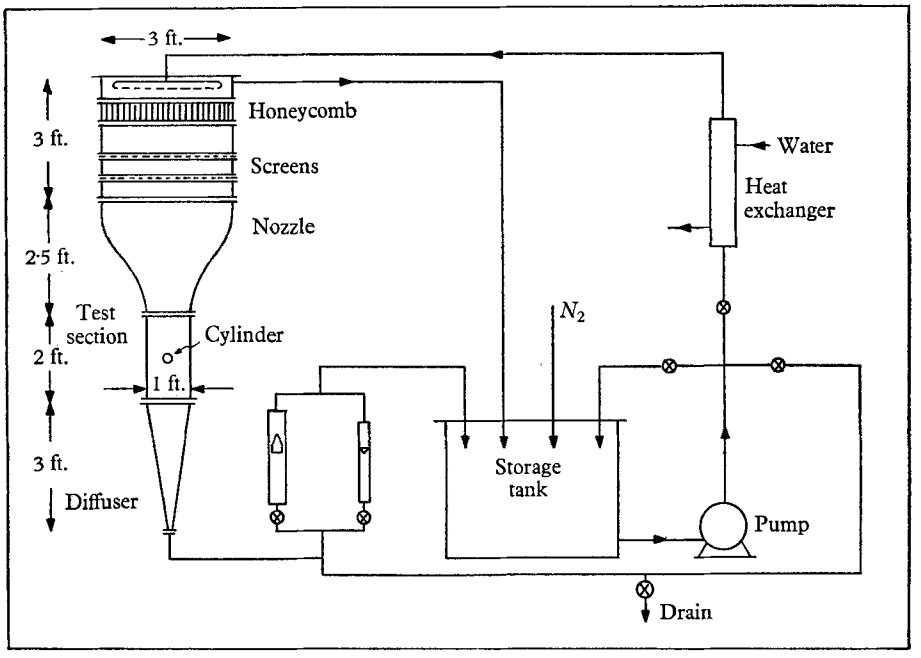

FIGURE 1. Sketch of the flow loop.

hour before each run. The ferricyanide ion is reduced to ferrocyanide ion at the cathode while the reverse reaction occurs at the anode. In the velocity gradient measurements the cathode was the test electrode while in the mass transfer studies it consisted of both the test electrode and the test cylinder. The anode was a piece of platinum foil located in the diffuser. The electric circuits were similar to those used by Mitchell & Hanratty (1966). A voltage of 0·5 V was applied across the electrodes. The current flowing in the cell was measured as a voltage drop across a standard resistor by means of a vacuum tube voltmeter. Fluctuating signals were time averaged by integration.

4. Character of the flow

Because of the very low velocities used in the test tunnel extra effort was necessary to insure that the flow was regular. This included special precautions in the design of the liquid distributer at the top of the tunnel and with respect to allowing the system to come to temperature equilibrium.

In all of the runs reported in this paper for the 0·020 in. × 0·500 in. electrode the signal was reasonably steady for locations prior to the separation region. However, after separation, and both in the presence and in the absence of the

splitter plate, the signal showed a random variation of very low frequency, of the order of one cycle/min. The characteristic time of this variation was much larger than the ratio d/u_∞ ($\sim$ 5 sec) and it was therefore presumed that at any instant this unsteadiness could be described by a pseudo steady-state hypothesis. It was found that this random variation occurred even when the tunnel was operated without discharging liquid into its top. It is therefore thought that the unsteadiness arose from disturbances downstream of the cylinder, probably caused by its wake.

In the experiments without a splitter plate the signals taken with the 0·020 in. $\times$ 0·500 in. electrode in the wake showed in addition a rather regular fluctuation whose period increased with Reynolds number. The Strouhal number for this rather regular disturbance was of the order of 0·18. This unsteadiness is believed to be due to the periodic shedding of vortices from the wake.

A number of recordings were also made of the signal from the circular 0·020 in. diameter test electrode in the cylinder used in the mass transfer studies. Signals obtained when only the test electrode was active were qualitatively the same as those for the 0·020 in. $\times$ 0·500 in. electrode in an inert cylinder. When the entire cylinder was active the circular test electrode gave quite a different behaviour. In the front half of the cylinder the signals did not appear to be as sensitive to flow disturbances as when the cylinder was inactive. However, in the back half of the cylinder the signal varied haphazardly with time with a much larger amplitude (compared to the time averaged signal) than was observed when the entire cylinder was not transferring mass. It is believed that these fluctuations were the result of natural convection effects, possibly caused by the shedding of the concentration boundary layer.

5. The measurements of wall velocity gradient

Measurements of the velocity gradient at the wall were obtained over a Reynolds number range of 60 to 332 without a splitter plate and of 115 to 339 with a splitter plate. These results are presented in table 1 as shear stresses since the viscosity of the fluid is known. The results for the rear portion of the cylinder are not presented for a Reynolds number of 60 since the corrections for natural convection and streamwise diffusion were too large.

Typical shear stress distributions with and without the splitter plate are shown in figures 2 and 3, where the ordinate is a dimensionless normalized velocity defined as

$$X = \frac{d}{2u_\infty}\frac{\beta_0}{R^{\frac{1}{2}}}.$$

It is noted that there is little difference between the results with and without a splitter plate. The electrochemical measurements indicate only the magnitude of the shear stress and not its sign. Therefore the assignment of positive and negative signs involves, to a certain extent, preconceived notions regarding the general pattern of the flow. In considering the results it was assumed that there existed only one separation point at which the shear stress is zero. It would also have been possible to interpret some of the profiles in the rear of the cylinder in

such a manner that there are more than one separation point. The profiles that resulted from such an interpretation did not seem reasonable in that they indicated changes in the wall velocity gradient in the rear of the cylinder that seemed

	Without a splitter plate		With a splitter plate	
	$R = 332$	$R = 104$	$R = 339$	$R = 115$
θ	$\tau_0 \times 10^5$	$\tau_0 \times 10^5$	$\tau_0 \times 10^5$	$\tau_0 \times 10^5$
5	4·68	0·62	4·45	0·54
10	10·1	1·13	9·23	1·07
15	14·2	1·82	13·3	1·54
20	17·5	2·40	17·0	1·95
25	23·4	3·08	20·5	2·32
30	25·2	3·50	23·5	2·70
35	27·1	3·85	26·1	2·97
40	29·0	4·24	27·2	3·16
45	30·3	4·65	27·8	3·28
50	30·4	5·00	27·8	3·31
55	30·0	—	27·2	3·30
60	28·7	4·97	26·0	3·11
65	27·1	4·53	24·0	2·86
70	23·8	4·08	20·9	2·59
75	19·7	3·44	16·6	2·34
80	16·7	3·03	13·5	2·03
85	12·2	2·77	9·74	1·73
90	6·99	2·33	5·88	1·41
95	3·52	1·82	3·45	1·13
100	2·26	1·49	1·55	0·88
105	0·67	1·12	0·37	0·66
110	−0·78	0·73	−0·74	0·47
115	−1·23	0·55	−1·25	0·32
120	−1·61	0·38	−1·45	0·18
125	−1·67	0·26	−1·31	0·11
130	−1·53	0·22	−1·14	−0·15
135	−1·25	−0·20	−1·01	−0·17
140	−1·05	−0·28	−0·87	−0·16
145	−0·65	−0·27	−0·78	−0·12
150	−0·63	−0·26	−0·73	−0·11
155	−0·70	−0·23	−0·68	−0·11
160	−0·67	−0·18	−0·63	−0·11
165	−0·32	−0·17	−0·54	−0·11
170	−0·42	−0·18	−0·39	−0·12
175	−0·43	−0·17	−0·25	−0·13
180	−0·32	−0·13	−0·14	−0·13
	$\mu = 1{\cdot}13$ cP	$\mu = 1{\cdot}13$ cP	$\mu = 1{\cdot}105$ cP	$\mu = 1{\cdot}01$cP
	$d = 2{\cdot}54$ cm		$\rho = 1{\cdot}042$ g mass/cm^3	

TABLE 1. Shear stress (gm force/cm^2) distributions.

too sudden. The separation angles determined by drawing a smooth curve through the data are shown in figure 4 and are in reasonable agreement with results already reported in the literature (Grove *et al.* 1964).

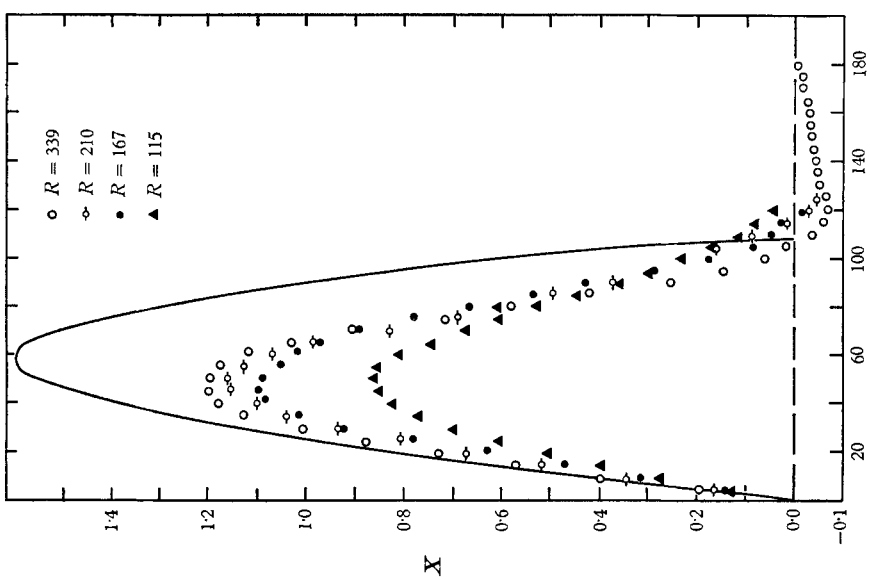

FIGURE 3. Shear stress variation around a cylinder with a splitter plate.

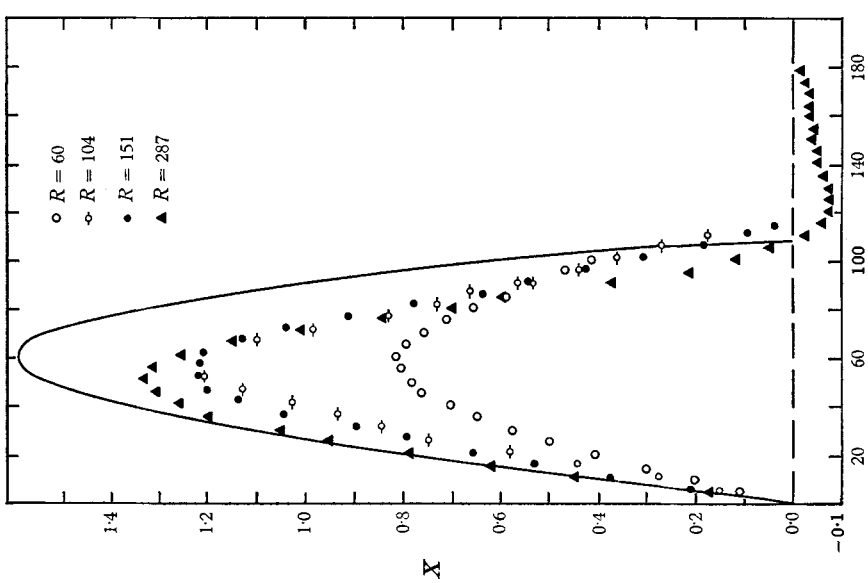

FIGURE 2. Shear stress variation around a cylinder without a splitter plate.

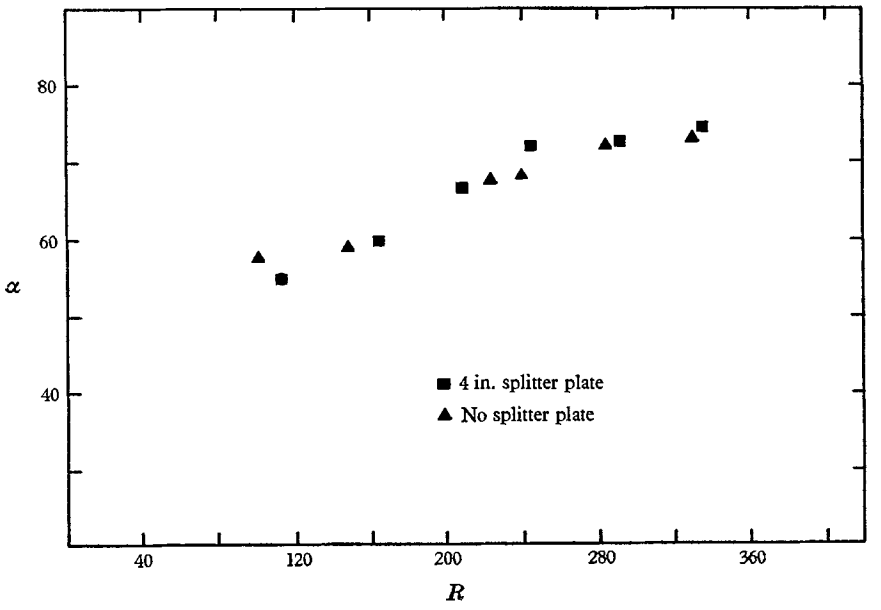

FIGURE 4. Separation angles obtained from measured shear stress distributions. α = separation angle from the rear stagnation point.

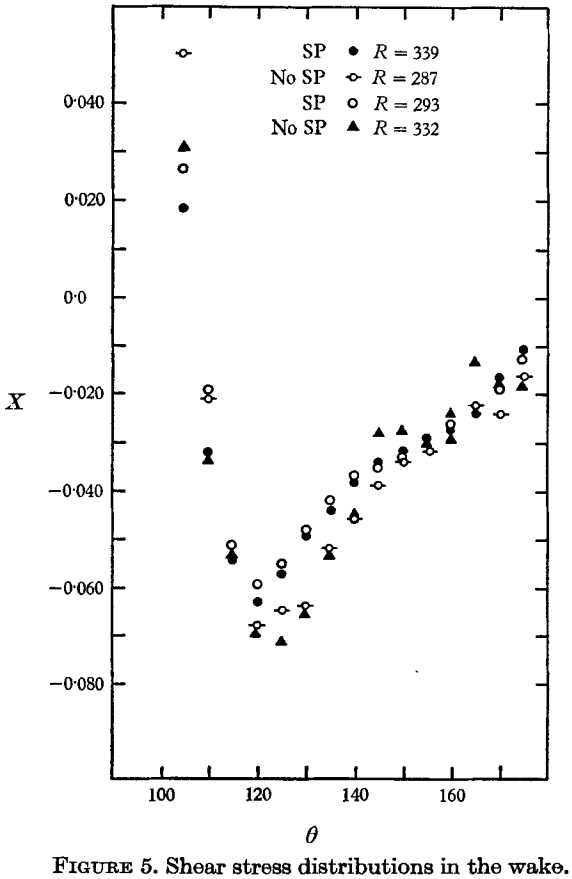

FIGURE 5. Shear stress distributions in the wake.

The wall velocity gradients in the rear of the cylinder are noted to be much smaller than those in the front. Typical measurements in this region are plotted in figure 5 in a much more expanded scale than is used in figures 2 and 3. The close agreement between the results with and without a splitter plate are of interest because of the apparent differences in the character of the flow in the wake for these two cases. The striking feature of these measurements is that the minimum shear stress is located close to the separation point. This result is quite different from the calculation by Kawaguti & Jain (1966) at a Reynolds number of 40, which gave the angle for the minimum as being approximately midway between the separation point and the rear stagnation point.

A few measurements of the shear stress were made with a circular test electrode of diameter 0·020 in. embedded in a 1 in. cylinder. The character of the unsteady signals and the magnitude of the signal at the wall in the rear of the cylinder are close to those obtained for the electrode with a width of 0·500 in. Likewise measurements using an electrode with a width of 1·00 in. showed no differences. These results with electrodes of different widths are consistent with the interpretation that the unsteadiness observed in the rear of the cylinder is the result of two-dimensional changes of a very low frequency which can be described by a pseudo-steady state approximation.

6. Local rates of mass transfer

The measurements of the variation of the local mass transfer rate around the cylinder are correlated in figure 6 using the Sherwood number $Sh = kd/u_\infty$. In these experiments mass transfer was occurring over the whole cylinder surface. The concentration boundary layer starts at the front stagnation point and thickens as it proceeds around the cylinder. Therefore, the mass transfer rate decreases with increasing θ.

It is of interest to compare these mass transfer results with calculations based on the measured velocity gradients. In these calculations it was assumed that there is only one separation point and that the flow in the wake close to the wall is two-dimensional. Mass transfer rates in the front half of the cylinder up to separation were calculated from (4) with $x = 0$ as the front stagnation point and those in the back half were calculated with $x = 0$ as the rear stagnation point. For these calculations the measurements of the velocity gradients were fitted with curves of the form

$$X = \sum_{m=1}^{5} b_m \sin m\theta. \tag{13}$$

It was found that the results were very sensitive to values of the slopes of the fitted curves at $\theta = 0°$ and at $\theta = 180°$.

The calculated mass transfer rates are shown in figure 7. The calculations for the rear of the cylinder must be accepted with some reservations since the use of (4) implies that a concentration boundary layer exists which is thin enough that the velocity profile may be represented by (3) and that the concentration external to the concentration boundary layer equals c_B. These assumptions could be in error in the rear portions of the cylinder.

With the exception of a Reynolds number of 115, the calculated and measured mass transfer rates agree within the accuracy to be expected from the calculations or from the measurements.

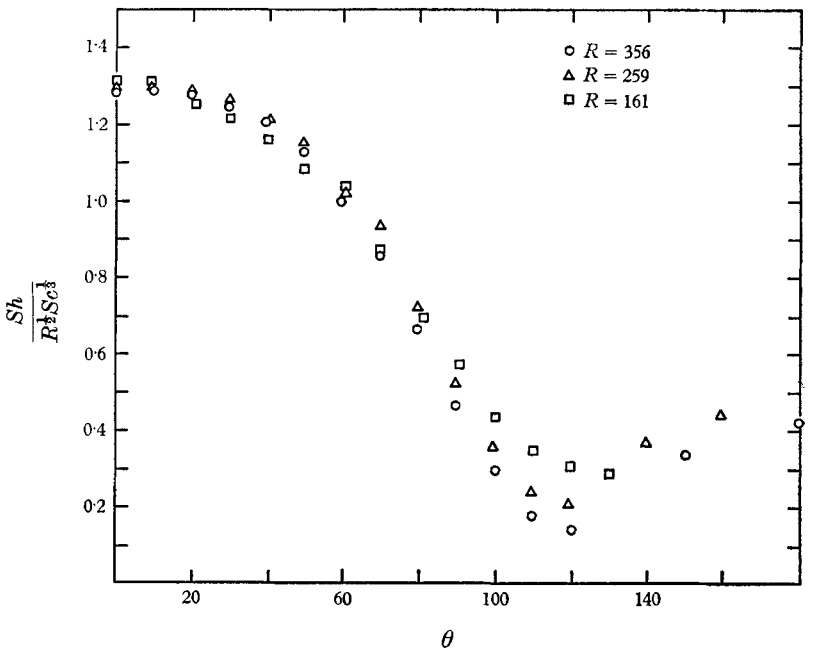

FIGURE 6. Variation of the local mass transfer rate.

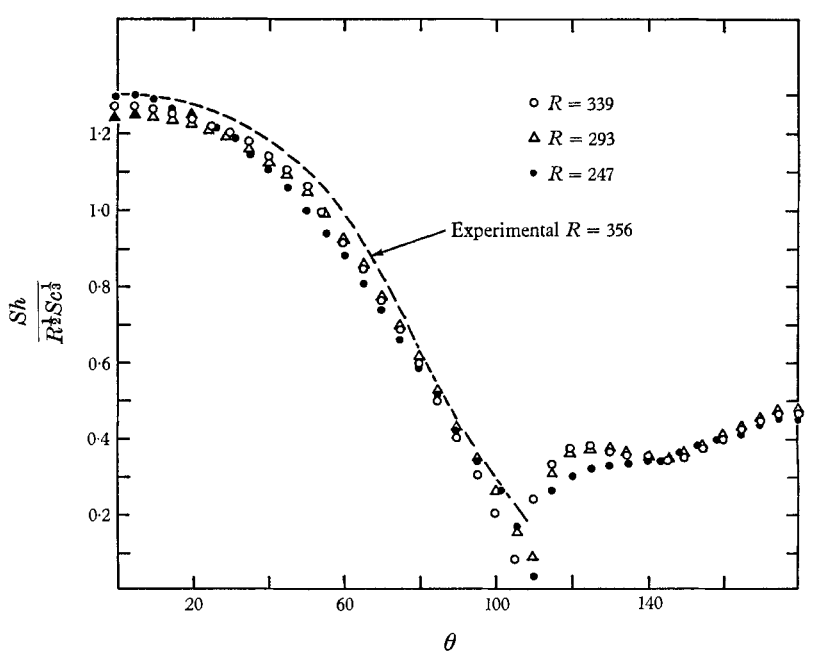

FIGURE 7. Mass transfer variation predicted from the measured distribution of shear stress.

The measurements at $R = 115$ were about 20% larger in the front regions of the cylinder than the calculations. This difference could be explained if the measurements of the velocity gradient were in error. A more reasonable explanation is that the mass transfer changed the flow field. Natural convection could be affecting the flow directly or indirectly through its influence on the pressure variation over the surface of the cylinder.

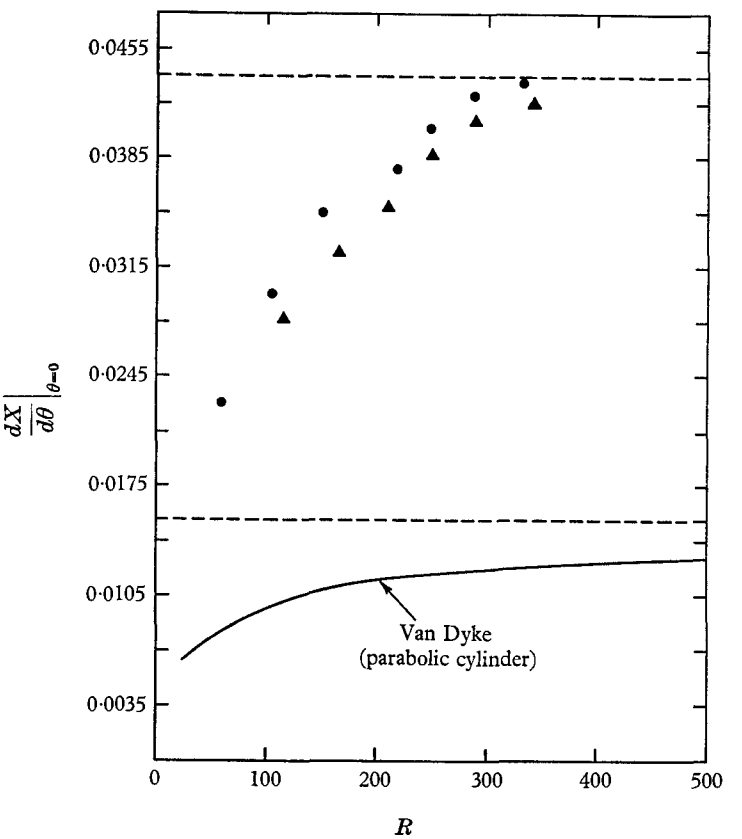

FIGURE 8. Effect of Reynolds number on the shear stress variation at the front stagnation point. ▲, with splitter plate; ●, without splitter plate.

Because of the large variations with time, it was quite difficult to obtain time-averaged mass transfer rates in the rear of the cylinder. Also there was some concern as to the meaning of such measurements. Therefore only a few mass transfer results in the rear of the cylinder are reported in figure 6. They were obtained from strip chart recordings of about 15 minutes duration. It is of interest, and perhaps surprising, that these results are also in agreement with calculations based on the measured velocity gradients in the rear of the cylinder.

The main conclusion to be drawn from the results reported in this section is that the measurements of the local mass transfer rates and of the velocity gradients at the wall are self consistent.

7. Comparison with boundary-layer theory

The solution of boundary-layer equations using a pressure distribution calculated from potential flow (see Schlichting 1960, p. 146) is indicated by the solid line in figures 2 and 3. This solution appears to describe measured velocity gradients in the neighbourhood of $\theta = 0°$ at large Reynolds number. Figure 8 is a plot of the rate of change of the velocity gradient at $\theta = 0°$ evaluated from the measurements. It is seen that agreement with the predictions for $R \to \infty$ is obtained for $R > 300$. For comparison the calculation by Van Dyke (1964) for a parabolic cylinder is also presented. The measurements for a circular cylinder depart much more suddenly from the solution for $R \to \infty$ than is indicated by the calculation for a parabolic cylinder. This difference could result in part from the differences in the systems but it also could result from the need to include more terms in the asymptotic expansions used by Van Dyke.

	Reynolds numbers			
	Thom			Kawaguti
	174	67	45	40
a_0	1·072	1·124	1·165	1·005
$a_2 \times 10^4$	−8·003	−6·226	−6·090	−7·394
$a_4 \times 10^8$	10·592	5·808	5·599	9·698
$a_6 \times 10^{12}$	−6·240	−1·571	−1·496	−6·048
$a_8 \times 10^{16}$	1·752	−0·382	−0·374	1·985
$a_{10} \times 10^{20}$	−0·207	0·257	0·251	−0·330
$a_{12} \times 10^{24}$	0·005	−0·034	−0·033	0·022

TABLE 2. Coefficients to equation (14)

An examination of the effect of Reynolds number on the distributions shown in figures 2 and 3 gives some indication of the limitations of boundary-layer theory. If boundary-layer theory is applicable and if the pressure distribution, normalized with respect to ρu_∞^2, is not changing with Reynolds number, the results for the front part of the cylinder as plotted in figures 2 and 3 should not be a function of Reynolds number. The shear stress distribution changes strongly in the range $60 < R < 115$ without a splitter plate and in the range $115 < R < 167$ with a splitter plate. The measured pressure profiles that have been reported in the literature do not change sufficiently over this range of Reynolds numbers to account for these variations. It is therefore concluded that boundary-layer theory becomes inaccurate in the range $60 < R < 105$ without a splitter plate and in the range $115 < R < 167$ with the splitter plate.

Thom (1933) has presented pressure measurements in the absence of a splitter plate for Reynolds numbers of 45, 67 and 174. These have been fitted by the least-squares technique to a polynomial of the form

$$\frac{p - p_\infty}{\frac{1}{2}\rho u_\infty^2} = \sum_{n=0}^{6} a_{2n} x^{2n}. \tag{14}$$

The constants in this series are given in table 2. The Blasius series solution (Rosenhead 1963) was used to calculate the profiles shown in figure 9. It is to be noted that boundary-layer theory predicts a much smaller change in the profiles with Reynolds number than is indicated by the measurements shown in figure 2.

The measurements at $R = 151$ are also presented in figure 9. Good agreement is obtained between experiments and boundary-layer theory. This agreement is evidence for the accuracy of the experimental techniques described in this paper.

The only other results on shear stress profiles around a cylinder are the calculations of Kawaguti & Jain (1966). It was therefore decided to use their pressure distribution and boundary-layer theory to calculate the shear stress distribution.

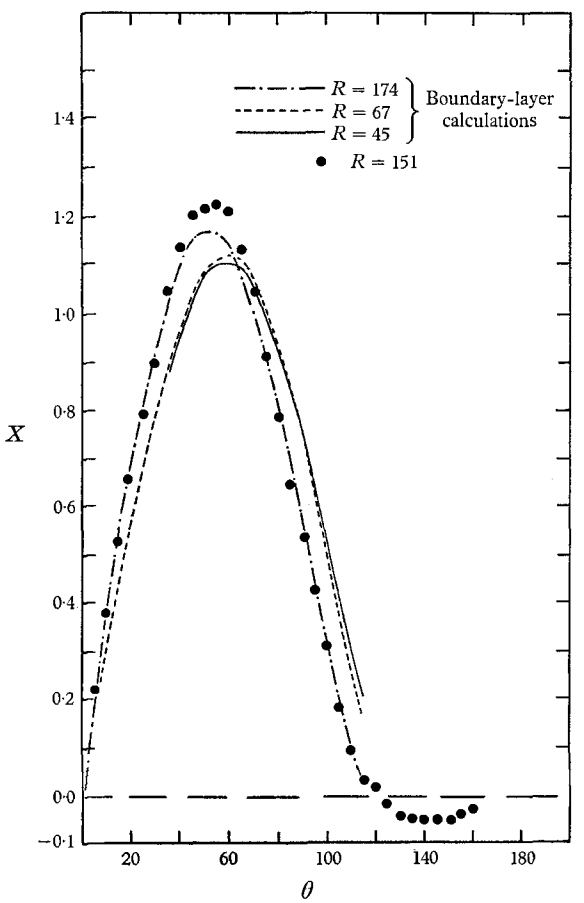

FIGURE 9. Comparison between boundary-layer calculations and measurements.

The constants in the series used to fit their pressure profile are presented in table 2 and the results of the calculation are presented in figure 10. It is seen that boundary-layer theory is in error. However, the error is not as large as would be indicated by the measurements reported in this paper. This could be explained by differences in the wake and external flow in the Kawaguti problem and in our experiments or by errors in the finite difference calculations.

8. Discussion of results in the wake

Grafton (1963) has suggested that the flow close to the wall in the wake could be represented by boundary-layer analysis. An attempt was made to calculate the shear stresses in the wake from the pressure measurements of Thom (1933). The results so far have been inconclusive since the calculations have been too sensitive to the accuracy of the fit of (14) to the pressure measurements.

Acrivos, Snowden, Grove & Petersen (1965) have made a proposal which is

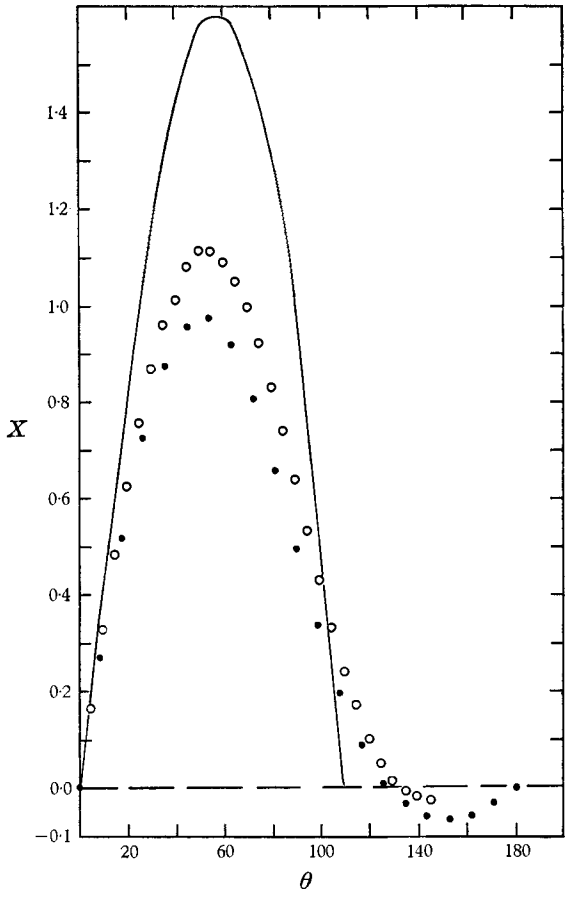

FIGURE 10. Calculations of Kawaguti at $R = 40$. ●, Kawaguti's numerical solution at $R = 40$. ○, boundary-layer solution using Kawaguti's numerical pressure distribution at $R = 40$.

quite different from that of Grafton. They argue that the entire wake bubble is a region in which viscous effects are of the same order as inertial effects. They conclude that the wall shear stress and Sherwood number in the wake would be independent of u_∞ for large Reynolds numbers. Shear stress data in the rear of the cylinder are plotted as a function of $R^{\frac{1}{2}}$ in figure 11. It is seen that the velocity gradient is being affected by the changes in R. Only at the rear stagnation point

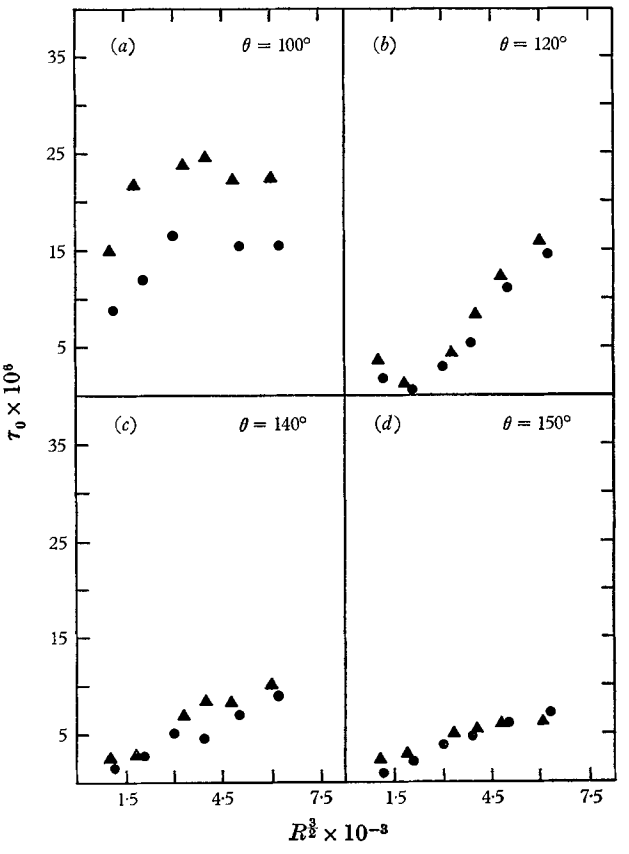

FIGURE 11. Effect of Reynolds number on the local shear stress in the rear of the cylinder. ▲, without splitter plate; ●, with splitter plate.

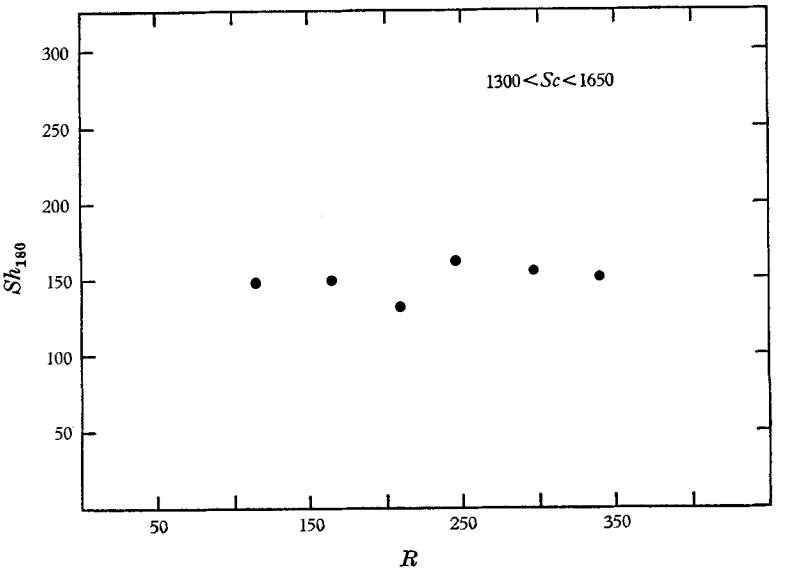

FIGURE 12. Mass transfer rate at the rear stagnation point for a cylinder with a splitter plate.

was it noted that the signal to the electrode is independent of R. These results are shown as a plot of Sh versus R in figure 12. This comparison with the prediction of Acrivos *et al.* could be unfair since it is quite possible that the experiments were not performed at high enough Reynolds numbers to be representative of the behaviour of the wake for $R \to \infty$.

Acknowledgment is made to the donors of the Petroleum Research Fund, administered by the American Chemical Society, for partial support of this work. Support was also received from the Air Force Office of Scientific Research under Grant AFOSR 547.

REFERENCES

Acrivos, A. 1960 *Phys. Fluids*, **3**, 657.

Acrivos, A. 1966 *Chem. Eng. Sci.* **21**, 343.

Acrivos, A., Snowden, D. D., Grove, A. S. & Petersen, E. E. 1965 *J. Fluid Mech.* **21**, 737.

Bellhouse, B. J. & Schultz, D. L. 1966 *J. Fluid Mech.* **24**, 379.

Dimopoulos, H. G. 1968 Ph.D. Thesis, University of Illinois, Urbana.

Goldstein, S. 1938 *Modern developments in Fluid Dynamics.* Oxford University Press.

Grafton, R. W. 1963 *Chem. Eng. Sci.* **18**, 457.

Grove, A. S., Shair, F. H., Petersen, E. E. & Acrivos, A. 1964 *J. Fluid Mech.* **19**, 60.

Kawaguti, M. & Jain, P. 1966 *J. Phys. Soc. Japan*, **21**, 2055.

Ling, S. C. 1962 *J. Heat Transfer*, C**85**, 230.

Mitchell, J. E. & Hanratty, T. J. 1966 *J. Fluid Mech.* **26**, 199.

Reiss, L. P. & Hanratty, T. J. 1962 *A.I.Ch.E. J.* **8**, 245.

Reiss, L. P. & Hanratty, T. J. 1963 *A.I.Ch.E. J.* **9**, 154.

Rosenhead, L. 1963 *Laminar Boundary Layers.* Oxford University Press.

Schlichting, H. 1960 *Boundary Layer Theory.* 4th edn. New York: McGraw Hill.

Son, J. S. 1968 Ph.D. Thesis in Chemical Engineering, University of Illinois, Urbana.

Thom, A. 1933 *Proc. Roy. Soc.* A **141**, 651.

Van Dyke, M. 1964 *J. Fluid Mech.* **19**, 145.